Robustness of the biaxial charge density wave reconstructed electron pocket against short-range spatial antiferromagnetic fluctuations

N. Harrison

Phys. Rev. B **97**, 245150 — Published 29 June 2018

DOI: 10.1103/PhysRevB.97.245150

Robustness of the biaxial charge-density wave reconstructed electron pocket against short-range spatial antiferromagnetic fluctuations

N. Harrison[1]
[1]*Mail Stop E536, Los Alamos National Labs.,Los Alamos, NM 87545*

Recent experiments on underdoped high temperature superconductors have shown that a biaxial charge-density wave coexisting with antiferromagnetism is able to account for the hole doping-dependences of the Hall coefficient and the charge-density wave ordering vector. Owing to the loss of long range order over the range of hole dopings where charge-density waves are observed, however, antiferromagnetism poses a serious challenge to the viability of Landau quantization and quantum oscillations. Here we make the surprising finding that the states along the antiferromagnetic Brillouin zone boundary, which are usually the most heavily broadened by antiferromagnetic fluctuations, become gapped once the biaxial charge-density wave forms. This gapping along with the location of the electron pocket produced by Fermi surface reconstruction at a momentum-space point of high symmetry causes the single nodal electron pocket to be largely protected against antiferromagnetic fluctuations in strong magnetic fields, enabling resolved Landau levels and quantum oscillations to remain robust against antiferromagnetic correlation lengths as short as $\sim$ 10 Å.

I. INTRODUCTION

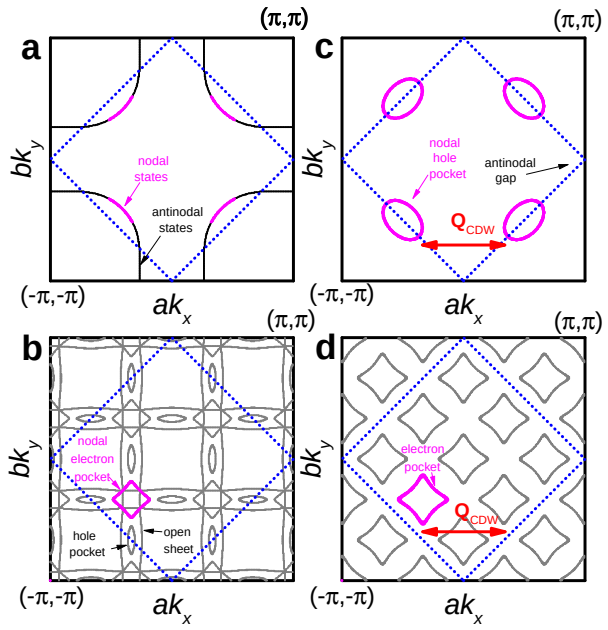

FIG. 1: (**a**), Schematic unreconstructed Fermi surface with the nodal (magenta) and antinodal (black) regions indicated. A blue dotted line indicates the antiferromagnetic Brillouin zone boundary. (**b**), Schematic Fermi surface reconstructed by bidirectional charge-density wave order showing that the nodal states become a diamond-shaped electron pocket (magenta) while the antinodal states become small hole pockets and open sheets (grey). (**c**), Schematic antiferromagnetic reconstructed Fermi surface consisting of hole pockets (magenta) intersected by the antiferromagnetic Brillouin zone boundary. (**d**). Schematic reconstructed Fermi surface due to coexisting antiferromagnetic and biaxial charge-density wave orders, showing that the states along the antiferromagnetic Brillouin zone are gapped.

A preponderance of experiments in the underdoped high temperature superconducting cuprates, including x-ray scattering,[1–3] magnetic quantum oscillations,[4–6] ultrasound,[7] angle-dependent magnetoresistance[8] and thermopower,[9] suggest that the Fermi surface is reconstructed by a biaxial charge-density wave at low temperatures and high magnetic fields. Reconstruction of the large Fermi surface predicted by band structure (see Fig. 1a) is proposed to lead to the creation of a small diamond-shaped electron pocket in high magnetic fields (shown in magenta in Fig. 1b),[10–13] which can account both for the low frequency observed in quantum oscillation experiments[14–16] and the sign and magnitude of the Hall coefficient.[17] Despite the recent success of the biaxial charge-density wave scheme in accounting for the reconstruction of the states in the nodal region of the Brillouin zone, it is becoming increasingly clear from combined angle-resolved photoemission and x-ray scattering studies[18–21] that a biaxial charge-density wave is unlikely to be responsible for producing the pseudogap in the antinodal region of the Brillouin zone.[22] Instead of producing a pseudogap, a biaxial charge-density wave has been shown to reconstruct the antinodal states into open sheets and small hole pockets (indicated in light grey in Fig. 1b).[11,12]

One widely held view is that the pseudogap is of similar origin to the Mott insulating state at zero hole doping, with the dominant interaction within the pseudogap regime being the antiferromagnet exchange between adjacent Cu sites.[30] In such a scenario, the starting Fermi surface consists of small hole pockets (similar to those depicted in magenta in Fig. 1c), which are then subject to a charge-density wave instability.[23–26] Biaxial charge-density wave Fermi surface reconstruction continues to produce a diamond-shaped electron pocket (shown in magenta in Fig. 1d), but without open sheets and small hole pockets being present.[23–26] Advantages of such a scheme are that it can be easily reconciled both with the hole doping-dependence of the Hall coefficient[27–29] (prior to formation of the charge-density wave phase)

and the doping-dependence of the charge-density wave ordering vector.[23–26] A serious disadvantage, however, is that the absence of long range antiferromagnetic order causes quasiparticle states in the vicinity of the antiferromagnetic Brillouin zone boundary (indicated by a blue dotted line in Fig. 1) to be heavily broadened, which appears to be in contradiction with the observation of sharp Landau levels in strong magnetic fields.[31,32]

As a first step towards understanding the effect of antiferromagnetic fluctuations on the reconstructed Fermi surface produced by a biaxial charge-density wave, we consider the simple case in which coexisting antiferromagnetic order is subject to spatial fluctuations of the ordering vector.[31–33] By opening a gap, a biaxial charge-density wave quenches what would otherwise be heavily broadened states at the antiferromagnetic Brillouin zone boundary (i.e. the dotted blue line in Fig. 1d). The reconstructed diamond-shaped electron pocket is therefore largely protected against antiferromagnetic fluctuations. We show this to be a crucial ingredient for the realization of sharp Landau and quantum oscillations in strong magnetic fields.

A key finding of our numerical simulations is that the energy broadening $\tilde{\Gamma}^{\rm e}_{\mu}$ of the electron pocket Landau level states is an order of magnitude lower than that $\tilde{\Gamma}^{\rm h}_{\mu} \approx \hbar v_{\rm F}/\xi$ previously estimated for nodal hole pockets[31,32] (where $v_{\rm F}$ is the Fermi velocity). $\tilde{\Gamma}^{\rm e}_{\mu}$ is further reduced by orbital averaging in strong magnetic fields. The creation of a coherent electron pocket Fermi surface may therefore be an important factor in the stabilization of biaxial charge-density wave order in strong magnetic fields. Using ξ values obtained from neutron scattering and nuclear magnetic resonances measurements, we find our numerical estimates of $\tilde{\Gamma}^{\rm e}_{\mu}$ and charge-density wave correlation length $\xi_{\rm CDW}$ to be consistent with their corresponding experimentally determined quantities in $YBa_2Cu_3O_{6+x}$ and $HgBa_2CuO_{4+\delta}$.

II. THE MODEL

We consider a recently considered scenario[23,25] in which a biaxial charge-density wave with ordering vectors $\mathbf{Q}_{{\rm CDW},x} = [\frac{2\pi\delta}{a}, 0]$ and $\mathbf{Q}_{{\rm CDW},y} = [0, \frac{2\pi\delta}{b}]$ coexists with antiferromagnetism whose ordering vector is $\mathbf{Q}_{\rm AFM} = [\frac{\pi}{a}, \frac{\pi}{b}]$. We assume the antiferromagnetism to retain a large amplitude despite the loss of long range order beyond a hole doping of $p \approx 0.05$, with spatial fluctuations being described solely in terms of a probabilistic broadening of $\mathbf{Q}_{\rm AFM}$.[31,32] We further assume the antiferromagnetism to have a uniform coupling and the charge-density wave to be of d-wave form.[12] The antiferromagnetic and charge-density wave couplings used in the calculations (see Appendix) are the approximate smallest values capable of producing Fermi surfaces consisting of a single type of pocket in Fig. 2.

A. Fermi surface reconstruction

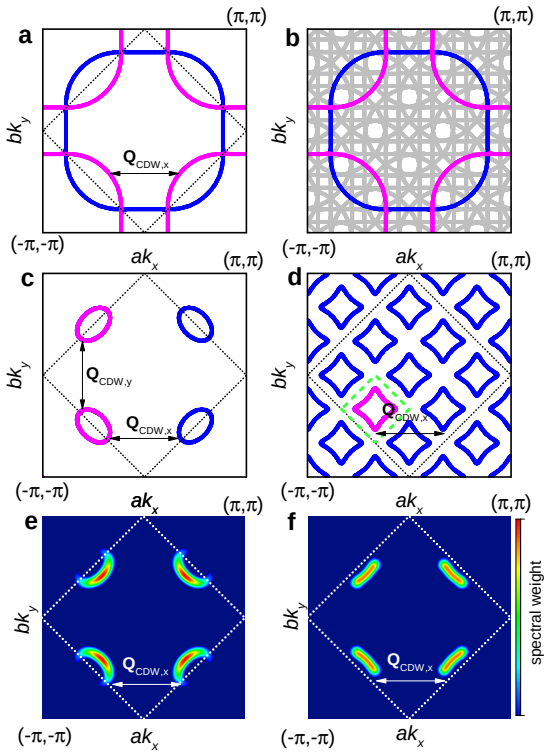

FIG. 2: (**a**), Schematic unreconstructed Fermi surface (magenta) of an underdoped cuprate for $p = 0.075$ and its copy (blue) translated by by the antiferromagnetic ordering vector $\mathbf{Q}_{\rm AFM}$. The antiferromagnetic Brillouin zone boundary is indicated by a dotted line. (**b**), Same as in (**a**) but with multiple copies (grey) translated by all possible summations and multiples of the charge-density wave ordering vectors $\mathbf{Q}_{{\rm CDW},x}$ and $\mathbf{Q}_{{\rm CDW},y}$, using $\delta = \frac{1}{3}$. (**c**), Reconstructed Fermi surface due to antiferromagnetic order consisting of two hole pockets (magneta) within the first Brillouin zone. (**d**), Reconstructed Fermi surface due to coexisting antiferromagnetic and charge-density wave order consisting of a single electron pocket (magenta) within the first Brillouin zone (igreen dashed line). (**e**), Simulated Fermi surface spectral weight for the antiferromagnetic order shown in (**c**), taking into consideration the effects of a short correlation length $\xi = 10$ Å. $A_{\mathbf{k},\omega,\sigma}$ from Equation (4) is convoluted with a Gaussian of width $\sigma = 0.015 \times 2\pi/a$ to simulate the experimental resolution. (**f**), Simulated Fermi surface spectral weight for the coexisting antiferromagnetic and charge-density wave order shown in (**d**), again, taking into consideration the effects of a short antiferromagnetic correlation length and finite resolution. Details of the Fermi surface reconstruction are contained in the Appendix.

The reconstructed Fermi surface resulting from coexisting antiferromagnetic and biaxial charge-density wave order are calculated by diagonalizing a Hamiltonian consisting of nested matrices (see Appendix). Figure 2a shows the unreconstructed Fermi surface together with its copy translated by $\mathbf{Q}_{\rm AFM}$ while Figure 2b shows

the same unreconstructed Fermi surface with its copies translated by all combinations of $\mathbf{Q}_{\rm AFM}$, $\mathbf{Q}_{{\rm CDW},x}$ and $\mathbf{Q}_{{\rm CDW},y}$. Figures 2c and d show the reconstructed Fermi surfaces for antiferromagnetic order and coexisting antiferromagnetic and biaxial charge-density wave order, respectively. A single electron pocket is obtained in Fig. 2d provided the antiferromagnetic and charge-density wave couplings are of sufficient strength (see Appendix).

We assume the total number of carriers to be conserved upon reconstructing the Fermi surface, which results in these carriers being distributed across one or more reconstructed bands. In the case of coexisting antiferromagnetic and biaxial charge-density wave order, the total number of holes p per unit area contained within the hole pockets inside the antiferromagnetic Brillouin zone in Fig. 2c is equivalent to the total number of holes per unit area contained between the reconstructed Brillouin zone boundary (dashed green line) and electron pocket (magenta) in Fig. 2d. It has recently been shown that the conservation of carriers leads to[24]

$$\delta = \frac{1}{2} - \sqrt{\frac{1}{2}\left(\frac{p}{2} + \frac{A_{\rm e}}{A_{\rm UBZ}}\right) + d^2}, \qquad (1)$$

where $A_{\rm UBZ} = 4\pi^2/ab$ is the area of the unreconstructed Brillouin zone and $A_{\rm e}$ is the area of the electron pocket. Here, δ refers to the average of its value along the x and y directions while $d \ll \delta$ refers to half the difference in δ between the x and y directions. On considering a specific commensurate case in which $\delta = \frac{1}{3}$ and $d = 0$ in Fig. 2d, we obtain a single electron pocket whose corresponding quantum oscillation frequency $F = \frac{\hbar}{2\pi e} A_{\rm e} \approx 500$ T is similar to that observed in $YBa_2Cu_3O_{6+x}$[8] by using $p = 0.075$.

B. Short range antiferromagnetism

The very short ξ in the underdoped cuprates implies that antiferromagnetism by itself is unlikely to provide a viable means of Fermi surface reconstruction. A very short ξ implies the absence of a sharp discontinuity in momentum-space separating filled and empty hole pocket states. States in the vicinity of the antiferromagnetic Brillouin zone that are spanned by the antiferromagnetic wave vector in Fig. 2c are also expected to be subject to temporal antiferromagnetic fluctuations. When short range antiferromagnetism coexists with a biaxial charge-density wave, however, the charge-density wave takes over the primary role of producing a reconstructed Fermi surface pocket and accompanying sharp discontinuity in momentum-space between filled and empty states. The remaining role of the antiferromagnetism is then to produce an antinodal gap, and this can remain robust against the effects of a short ξ, provided the antiferromagnetic coupling is of sufficient strength. Since the biaxial charge-density wave gaps states along the antiferromagetic Brillouin zone boundary that are spanned by the antiferromagnetic wave vector in Fig. 2d, the effect of temporal antiferromagnetic fluctuations on the Fermi surface is also expected to be reduced.

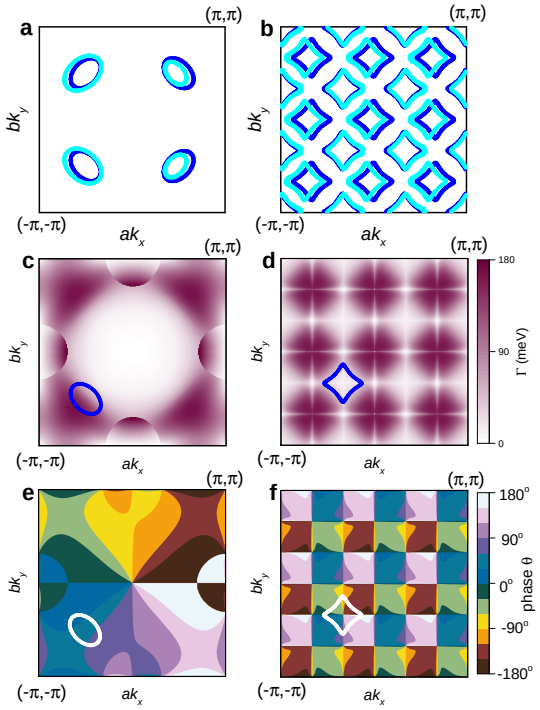

FIG. 3: (**a**), Reconstructed Fermi surface from antiferromagnetic order with (blue) overlaid with that including a small deviation $\mathbf{q}_{\rm AFM}$ of the ordering vector from $\mathbf{Q}_{\rm AFM}$ (cyan), using $q_x = 0.03 \times 2\pi/a$ and $q_y = 0$, which is equivalent to displacement in momentum-space of ξ^{-1} where $\xi = 20$ Å. (**b**), Same as (**a**), but for coexisting short range antiferromagnetic and charge-density wave order. (**c**), Magnitude of the broadening $\Gamma_{\mathbf{k},\mu}$ for the band closest to the chemical potential in the case of short range antiferromagnetic order, with the location of one of the hole pockets shown. (**d**), $\Gamma_{\mathbf{k},\mu}$ for the band closest to the chemical potential in the case of coexisting short antiferromagnetic and charge-density wave order, with the location of one of the electron pockets shown. Corresponding $\Gamma_{\mathbf{k},\mu}$ may be several times lower in practice, owing to the renormalization of the bands required to reproduce the experimental effective mass. (**e**), Color-coded approximate phase $\theta_{\mathbf{k},\mu}$ of the broadening for short range antiferromagnetic order. (**f**), Corresponding $\theta_{\mathbf{k},\mu}$ for coexisting short antiferromagnetic and charge-density wave order.

To model the effect of quasi-static short range antiferromagnetic order, we consider the fact that a small deviation $\mathbf{q}_{\rm AFM} = [q_x, q_y]$ of the antiferromagnetic ordering vector from its mean value $\mathbf{Q}_{\rm AFM}$ causes a small shift in the reconstructed Fermi surface (see Figs. 3a and b). As previously considered elsewhere,[32] we assume these deviations to be subject to a Lorentzian probability distribution of form

$$P(q_x, q_y) = \frac{1}{\pi^2} \frac{\xi^{-1}}{q_x^2 + \xi^{-2}} \frac{\xi^{-1}}{q_y^2 + \xi^{-2}}, \qquad (2)$$

yielding a k-dependent momentum-space broadening of

the electronic states. Such a form considers the periodicity of the antiferromagnetism to be subject to statistical broadening while its overall amplitude remains constant. Since the periodicity is given by the gradient of the phase, we must also assume that the phase varies linearly in space over distances of order the correlation length ξ. The symmetric form of the distribution function nevertheless implies that the phase of the antiferromagnetism averages to zero over very large distances.

When the reconstructed electronic bands are averaged according to Equation (2) over all possible values of q_x and q_y, the finite value of ξ causes the electronic states at fixed energy to be broadened in momentum-space, with the line shape having a Lorentzian form. One can equivalently consider the eigenstates at a fixed values of the momentum-momentum space vector $\mathbf{k}$ to be subject to a broadening in energy. The energy broadening has a Lorentzian line shape that varies as a function of $\mathbf{k}$, and this can calculated in a computationally efficient way from the gradient

$$\mathbf{\Gamma}_{\mathbf{k},\mu} \approx \frac{1}{\xi}\nabla\varepsilon_{\mathbf{k},\mu}(q_x, q_y). \tag{3}$$

The vectorial form of Equation (3) provides a means for keeping track the q_x and q_y contributions to the broadening, which can differ significantly for some values of $\mathbf{k}$. Below, we show that the orbitally-averaged direction of $\mathbf{\Gamma}_{\mathbf{k},\mu}$ can play an important role in protecting the electron-pocket against excessive Landau level broadening. The subscript μ refers to our considering only the band closest to the chemical potential μ.

1. Angle-resolved Photoemission

Since the photoemission spectral weight is a map of the intensity of electrons emitted from electronics states at different fixed values of the momentum vector $\mathbf{k}$, for its calculation we need only be concerned with the k-dependent magnitude $\Gamma_{\mathbf{k},\mu}$ of the broadening given by Equation (3). Figures 3c and d show the magnitude of the energy broadening calculated for antiferromagnetic order and coexisting biaxial change-density wave and antiferromagnetic orders, respectively.

Figs.2e and f show the photoemission spectral weight in the presence of broadening simulated using the convolution

$$A_{\mathbf{k},\omega,\sigma} = \frac{1}{\pi}\mathrm{Im(G)} \circledast \frac{1}{\pi}\frac{\Gamma_{\mathbf{k},\mu}}{(\varepsilon_\mu - \omega)^2 + \Gamma^2_{\mathbf{k},\mu}}, \tag{4}$$

where $\omega = 0$ refers to the Fermi surface. Here $\mathrm{G} = ((\omega + i\Gamma)I - H_{\mathbf{k}})^{-1}_{11}$ is the Green's function, Γ represents a small uniform broadening of the quasiparticle states (whose origin is distinct from ξ), I is the identity matrix, $H_{\mathbf{k}}$ represents the Hamiltonian $H^{\mathrm{AFM}}_{\mathbf{k}}$ or $H^{\mathrm{AFM+CDW}}_{\mathbf{k}}$ in the Appendix and the subscript 11 refers to the first element.

The calculated photoemission spectral weight in Fig. 2 produces 'Fermi arcs' for both antiferromagnetic and coexisting antiferromagnetic and charge-density wave orders. In the former case, the arc corresponds to one side of the hole pocket while in the latter it corresponds to one side of the diamond-shaped electron pocket. Whereas the calculated Fermi arc for short-range antiferromagnetic order closely resembles angle-resolved photoemission experimental results in underdoped $YBa_2Cu_3O_{6+x}$,[31,34] it overestimates the spectral weight along the boundary of the antiferromagnetic Brillouin zone. This excess spectral weight vanishes in Fig. 2f upon incorporating a coexisting biaxial charge-density wave into the simulation.

The charge-density wave ordering vectors span the separation between hole pockets resulting from antiferromagnetic Fermi surface reconstruction (see Fig. 2c) and also determine the periodicity of the electron pockets in the extended Brillouin zone scheme resulting from coexisting antiferromagnetic and charge-density wave Fermi surface reconstruction (see Fig. 2d). The charge-density wave vectors also span the separation between the Fermi arcs in Figs. 2e and f, as previously noted.[4,18,19]

2. Landau level broadening

Momentum-space broadening caused by short-range antiferromagnetism was previously shown to have an adverse affect on nodal hole pockets (e.g. those depicted in Fig. 2c),[31,32] with the Landau level broadening becoming too large for quantum oscillations to be observed once $\xi \lesssim 100$ Å. The extreme sensitivity of the hole pocket Landau level broadening to ξ originates from the location of the pocket along the antiferromagnetic Brillouin zone boundary, where its area is linearly dependent on q_x and q_y (see Fig. 3a). The statistical broadening given by Equation (2) leads to a distribution of areas $\Delta A_0 \approx A_{\mathrm{h}}\Gamma_{\mu,0}/\varepsilon_{\mathrm{F}}$ (valid for a quasi-two-dimensional closed pocket), where A_{h} is the area of the hole pocket and ε_{F} is the effective Fermi energy (the depth in energy to which states are filled within the pocket). Since the broadening is of the same Lorentzian form as that associated with the scattering of quasiparticles from defects and impurities,[35] one can consider an effective timescale, $\tau_\xi = \frac{\hbar}{2\Gamma_{\mu,0}}$, characterizing the distribution of times over which quasiparticles propagate before being affected by ξ. Here, $\Gamma_{\mu,0} = \int_0^{T_{\mathrm{c}}} \Gamma_{\mathbf{k},\mu}\mathrm{d}t$ corresponds to the magnitude $\Gamma_{\mathbf{k},\mu}$ averaged over one cyclotron orbit period $T_{\mathrm{c}} = 2\pi/\omega_{\mathrm{c}}$ in Fig. 3c, where $\omega_{\mathrm{c}} = eB/m^*$ is the cyclotron frequency and m^* is the quasiparticle effective mass. Lorentzian broadening causes the damping of the hole pocket quantum oscillations to acquire the standard exponential form,[35]

$$R^{\mathrm{h}}_\xi \approx \mathrm{e}^{-\frac{\pi}{\omega_{\mathrm{c}}\tau_\xi}}, \tag{5}$$

which is expected to be valid over a broad range of timescales. The limit $\tau_\xi > T_{\mathrm{c}}$ corresponds to a situation

in which the majority of cyclotron orbits lie within individual antiferromagnetic "domains" within which $\mathbf{q}_{\rm AFM}$ is approximately constant. The opposite limit $\tau_\xi < T_{\rm c}$, which is more applicable to the present case of a very short ξ, implies that $\mathbf{q}_{\rm AFM}$ remains constant only for a tiny fraction of cyclotron orbits.

In contrast to the hole pocket, the electron pocket in Figs. 3b and d is located at a point of high symmetry where its area depends only quadratically on q_x and q_y. Under circumstances where hole doping is conserved in response to perturbations in $\mathbf{Q}_{\rm AFM}$ by $\mathbf{q}_{\rm AFM}$, its area becomes independent of q_x and q_y, leading to a situation in which the orbital average of the magnitude $\Gamma_{\mathbf{k},\mu}$ is no longer adequate for estimating the Landau level broadening. The degree of Landau level broadening must instead be estimated from $\mathbf{\Gamma}_{\mathbf{k},\mu}$ orbitally averaged over the distribution of times $t - t_0$ for which the quasiparticles remain unaffected by ξ. The Lorentzian line shape of the broadened Landau levels implies that the probability of a quasiparticle propagating before being affected by ξ to time $t-t_0$ has an exponential form $P(t) = \frac{1}{2\tau_\xi} e^{-\frac{t}{2\tau_\xi}}$,[35] as is found to be the case for the scattering of quasiparticles from defects and impurities. The Landau level broadening is then given by the magnitude of the average of $\mathbf{\Gamma}_{\mathbf{k},\mu}$ over this probability distribution, requiring the following integration

$$\tilde{\Gamma}_\mu = \int_0^{\frac{2\pi}{\omega_{\rm c}}} \frac{\omega_{\rm c}}{2\pi} \left| \int_0^\infty \frac{1}{2\tau_\xi} e^{-\frac{t}{2\tau_\xi}} \mathbf{\Gamma}_{\mathbf{k},\mu}(t-t_0) {\rm d}t \right| {\rm d}t_0 \qquad (6)$$

over all possible time intervals $t-t_0$ and starting times t_0. For the electron pocket in Figs. 3d, we proceed to simplify the integration by considering an approximation $\mathbf{\Gamma}_{\mathbf{k},\mu} \approx \Gamma_{\mu,0}[\cos\omega_{\rm c}(t-t_0), \sin\omega_{\rm c}(t-t_0)]$ in which the magnitude $\Gamma_{\mathbf{k},\mu}$ is assumed to be constant while $\partial\theta_{\mathbf{k},\mu}/\partial t = \omega_{\rm c}$. On substituting this approximate form into Equation (6), we obtain

$$\tilde{\Gamma}^{\rm e}_\mu \approx \frac{1}{\sqrt{4\omega_{\rm c}^2\tau_\xi^2 + 1}} \Gamma_{\mu,0} \qquad (7)$$

for the electron pocket Landau level width. Orbital averaging therefore causes the width of the electron pocket Landau levels to undergo considerable narrowing in strong magnetic fields (see Fig. 4a). The corresponding electron pocket quantum oscillation damping factor therefore has the form

$$R^{\rm e}_\xi \approx {\rm e}^{-\frac{\pi}{\omega_{\rm c}\tau_\xi}\frac{1}{\sqrt{4\omega_{\rm c}^2\tau_\xi^2+1}}}, \qquad (8)$$

which is notably different from that obtained for the hole pockets.

The differences in behavior of hole and electron pockets can be understood by taking into consideration changes in the direction of $\mathbf{\Gamma}_{\mathbf{k},\mu}$ given by Equation (3) that occur on completing a cyclotron orbit. We represent this direction graphically in Fig. 3e and f by mapping the polar angle $\theta_{\mathbf{k},\mu}$, where $\mathbf{\Gamma}_{\mathbf{k},\mu} = \Gamma_{\mathbf{k},\mu}[\cos\theta_{\mathbf{k},\mu}, \sin\theta_{\mathbf{k},\mu}]$. For the hole pocket, $\mathbf{\Gamma}_{\mathbf{k},\mu}$ always points away from the antiferromagnetic Brillouin zone center, causing $\theta_{\mathbf{k},\mu}$ to change by only $\approx 45^\circ$ on completing a cyclotron orbit. The small change in angle gives rise to a magnitude of orbital average of $\mathbf{\Gamma}_{\mathbf{k},\mu}$ that is very similar in value to the orbital average of the magnitude $\Gamma_{\mathbf{k},\mu}$, justifying the use of the magnitude in deriving Equation (5) for the hole pocket. For the electron pocket, by contrast, $\theta_{\mathbf{k},\mu}$ sweeps out a full 360° on competing a cyclotron orbit. The large change in angle gives rise to a magnitude of the orbital average of $\mathbf{\Gamma}_{\mathbf{k},\mu}$ that is significantly reduced relative to the orbital average of the magnitude $\Gamma_{\mathbf{k},\mu}$.

III. NUMERICAL ESTIMATES OF THE BROADENING

The calculated broadening in Fig. 3 provides a basis from which we can numerically estimate the the extent of the Landau level broadening in the underdoped cuprates $YBa_2Cu_3O_{6+x}$ and $HgBa_2CuO_{4+\delta}$, and the degree to which it is suppressed by a magnetic field. The magnetic field-dependent broadening can then be used to estimate the quantum oscillation damping, and this can in turn be compared directly against quantum oscillation measurements. The antiferromagnetic correlation length ξ has previously been estimated in neutron scattering and nuclear magnetic resonance measurements.

A. Experimental estimates of ξ

In $YBa_2Cu_3O_{6+x}$, despite the loss of long range antiferromagnetic order for hole dopings $p \gtrsim 0.05$,[30] the imaginary susceptibility χ'' detected in neutron scattering experiments continues to exhibit a strong excitation (or resonance) at $\mathbf{Q}_{\rm AFM}$ with a correlation length of $\xi \approx 20$ Å.[30,36,37] The form of the imaginary susceptibility $\chi''(\omega)$ evolves from being completely gapped at excitation energies $\omega \lesssim 10$ meV at temperatures below $T_{\rm c}$, to having a form $\chi'' \propto \omega$ at temperatures above $T_{\rm c}$. The linear form is considered to be characteristic of a metallic state exhibiting diffusive spin dynamics.[30,38] Nuclear magnetic resonance studies further suggest a characteristic spin fluctuation frequency $\omega_{\rm sf}$ that lies between 2 and 3 meV for hole dopings near $p \approx 0.11$,[30,37] which coincides with the doping at which the quantum oscillation amplitude is observed to be largest.[4,39] At this doping, the cyclotron frequency $\omega_{\rm c}$ reaches a value of ≈ 7 meV in a magnetic field of 100 T. Since $\omega_{\rm c} > \omega_{\rm sf}$ in very strong magnetic fields, the low energy spin fluctuations may be regarded as being essentially 'quasistatic' from the perspective of orbiting quasiparticles.

In $HgBa_2CuO_{4+\delta}$, χ'' also exhibits a strong peak at $\mathbf{Q}_{\rm AFM}$, but at a higher excitation energy than in $YBa_2Cu_3O_{6+x}$ and with a shorter correlation length of $\xi \approx 10$ Å.[40] One significant departure of χ'' in $HgBa_2CuO_{4+\delta}$ from that observed in other cuprates

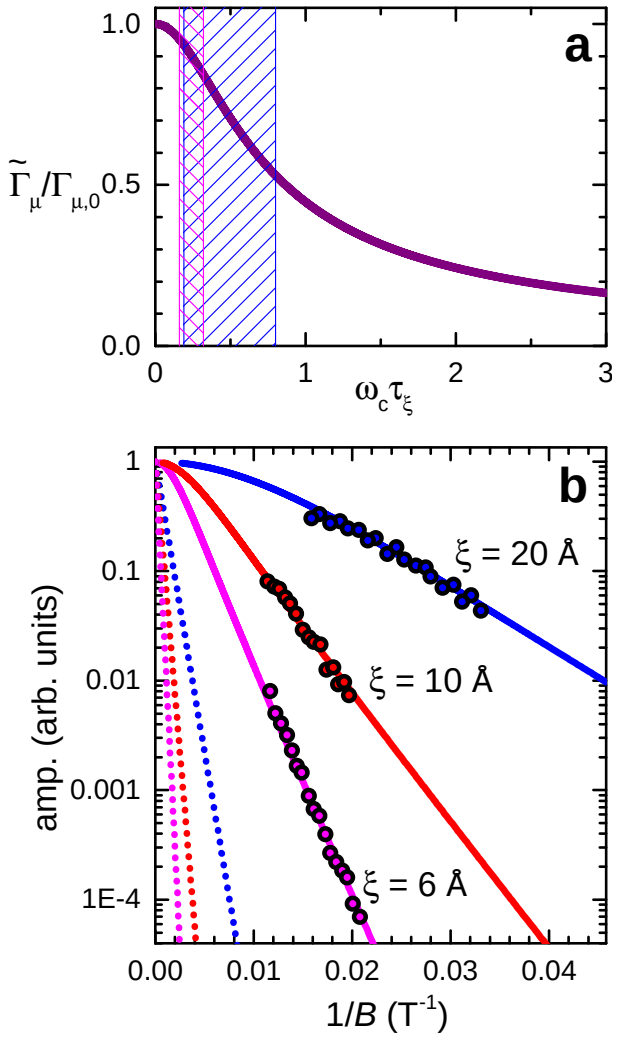

FIG. 4: (**a**), Calculated generic form for the magnetic field-dependent Landau level broadening $\tilde{\Gamma}_\mu$ (solid line) according to Equation (7). Shaded regions represent the range in magnetic field accessed in $YBa_2Cu_3O_{6+x}$ (blue) and $HgBa_2CuO_{4+\delta}$ (magenta). (**b**), Quantum oscillation damping calculated for $YBa_2Cu_3O_{6+x}$ (blue) and $HgBa_2CuO_{4+\delta}$ (magenta and red) according to Equation (8), using the parameters listed in Table I. The calculations are compared with experimental data from Refs.[6,41] plotted in the same colors. For the $HgBa_2CuO_{4+\delta}$ sample with a higher $T_c \approx 74$ K, a shorter antiferromagnetic correlations length of $\xi \approx 6$ Å is required to reproduce the steepness of the experimental 'Dingle plot.' For comparison, the dotted lines show the predicted quantum oscillation damping for the case of hole pockets (using the experimentally measured effective mass), where $\zeta_{\mu,0} \approx 0.91$ and $\Gamma_{\mu,0} = 28$ meV (blue), 56 meV (red) and 94 meV (magenta), respectively.

(such as $YBa_2Cu_3O_{6+x}$ and $La_{2-x}Sr_xCuO_{4-\delta}$[30,37,38]) is the reported persistence of the spin fluctuation gap at temperatures above T_c.[40] On the other hand, the low energy properties of χ'' in $HgBa_2CuO_{4+\delta}$ have yet to be investigated by means of nuclear magnetic resonance.

B. Landau level width

To compare numerical estimates of the quantum oscillation damping factor with those seen experimentally, we use the measured effective masses for converting between momentum-space and energy broadenings. In $YBa_2Cu_3O_{6+x}$, the electron pocket quasiparticle effective mass has been found to be $m^* \approx 1.6\ m_e$(where m_e is the free electron mass) for hole dopings near $p \approx 0.11$,[4] which is somewhat heavier than the band mass of $m_b = 0.57\ m_e$ obtained for our calculated Fermi surface depicted in Figs. 2 and 3. We assume this difference to be attributed to a renormalization of the quasiparticle bands.

We estimate the magnitude

$$\Gamma_{\mu,0} \approx \zeta_{\mu,0}\frac{\hbar^2 k_F \xi^{-1}}{m^*} \tag{9}$$

of the zero magnetic field energy broadening by assuming the proportionality $\Gamma_{\mu,0}/\varepsilon_F \approx \Delta A_0/A_e$ (valid for a quasi-two-dimensional closed pocket), where $\varepsilon_F = \hbar^2 k_F^2/2m^* = \hbar eF/m^*$ is the effective Fermi energy, $\Delta A_0 = 2\pi k_F \Delta k_0$ is the momentum-space area broadening and Δk_0 is the corresponding average magnitude of the width of the broadening perpendicular to the Fermi surface. We estimate $\Delta k \approx 0.035 \times k_F$ numerically for $\xi = 20$ Å by averaging the numerically calculated change in the radius of the electron pocket in Fig. 3b parallel to $[q_x, q_y]$ for different values of q_x and q_y (subject to the constraint $\sqrt{q_x^2 + q_y^2} = \pm\xi^{-1}$). The dimensionless quantity $\zeta_{\mu,0} = \xi\Delta k_0 \approx 0.088$ is our calculated estimate of the sensitivity of broadening of the electron pocket to ξ. Values for $\Gamma_{\mu,0}$ are tabulated in Table I, along with experimental estimates for ξ, F and m^*.

material	$YBa_2Cu_3O_{6+x}$	$HgBa_2CuO_{4+\delta}$
p	0.11	0.09
ξ	20 Å	10 Å
F	530 T	840 T
m^*	1.6 m_e	2.7 m_e
$\Gamma_{\mu,0}$	2.7 meV	4.0 meV

TABLE I: Tabulated values of the hole doping p, antiferromagnetic correlation length ξ, quantum oscillation frequency F and quasiparticle effective mass m^* used in the $\Gamma_{\mu,0}$ estimates.

Having obtained numerical estimates for $\Gamma_{\mu,0}$, we proceed to calculate the Landau level broadening in a magnetic field using Equation (7). Figure 4a shows $\Gamma_{\mu,0}$ plotted as a function of the dimensionless quantity $\omega_c\tau_\xi$, which is independent of m^*. The shaded regions indicate the range in $\omega_c\tau_\xi$ over which quantum oscillations have been observed experimentally. In $YBa_2Cu_3O_{6+x}$, the magnetic field range over which quantum oscillations are seen extends from $\approx$ 25 to 100 T,[4] suggesting that $\tilde{\Gamma}_\mu$ falls to as low as $\approx$ 1.3 meV in experiments. In $HgBa_2CuO_{4+\delta}$, the magnetic field range over

which quantum oscillations are seen extends from ≈ 45 to 90 T,[6] suggesting a larger minimum Landau level width of ≈ 3 meV.

C. Quantum oscillation damping

On calculating the quantum oscillation damping using Equation (8) (see Fig. 4b), we find that the short antiferromagnetic correlation lengths reported in neutron scattering and nuclear magnetic resonance experiments in $YBa_2Cu_3O_{6+x}$ and $HgBa_2CuO_{4+\delta}$ produce a magnetic field-dependent damping that is consistent with the slopes of the 'Dingle plots' obtained from quantum oscillation experiments.[6,41] Only the absolute amplitude 'prefactor' of the experimental data needs to be adjusted in order to bring the model into alignment with the experimental data points. The exception is the $HgBa_2CuO_{4+\delta}$ sample with a higher T_c of 74 K, which requires a significantly smaller antiferromagnetic correlation length of $\xi \approx 6$ Å.[6] For comparison, we indicate using dotted lines in Fig. 4b the much stronger damping from Equation (5) expected for the case of hole pockets.

D. Charge-density wave correlation length

In the case where the reconstructed Fermi surface consists of a single pocket, the reduction in the Landau level width with increasing magnetic field gives rise to a proportionate reduction in the the momentum-space area broadening $\tilde{\Delta A} = A_e\tilde{\Gamma}_\mu/\varepsilon_F$, which is therefore likely to be an important factor in stabilizing the biaxial charge-density wave ground state in high magnetic fields. To test for the existence of a direct relationship between ξ and the magnetic field-dependent charge-density wave correlation length ξ_{CDW}, we equate the electron pocket area broadening with that $\tilde{\Delta A} \approx k_{diag}\xi_{CDW}^{-1}$ associated with the finite charge-density wave correlation length ξ_{CDW} (see inset to Fig. 5). Here, $k_{diag} = \sqrt{2\pi}k_F$ is the length of the electron pocket diagonal in the inset to Fig. 5 (defining $k_F \approx \sqrt{A_e/\pi}$). On equating the broadening areas, we obtain

$$\xi_{CDW} \approx \xi\zeta_{\mu,0}^{-1}\sqrt{\frac{2}{\pi}(4\omega_c^2\tau_\xi^2+1)}. \qquad (10)$$

The calculated curve in Fig. 5 is found to be consistent with the experimentally measured values of ξ_{CDW} in $YBa_2Cu_3O_{6+x}$ (blue) and $HgBa_2CuO_{4+\delta}$ (magenta) in Fig. 5,[3,21,42] suggesting that a scenario in which the finite charge-density wave correlation length is limited by short range antiferromagnetic correlations appears to be plausible. In $YBa_2Cu_3O_{6+x}$, experiments have revealed two coexisting forms of charge-density wave in strong magnetic fields. One of these is present at zero magnetic field, is biaxial, is staggered between consecutive bilayers (i.e. $l = \frac{1}{2}$) and has a shorter correlation length while

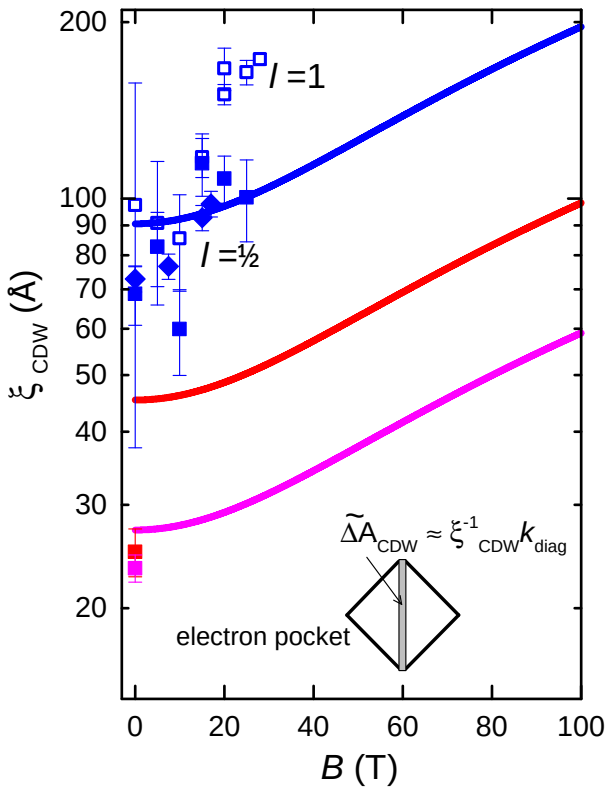

FIG. 5: Calculated charge-density wave correlation length according to Equation (10) for the different sample compositions and correlation lengths considered in Fig. 4. The curves are compared with experimental values of the $l = \frac{1}{2}$ charge-density wave correlation length for $YBa_2Cu_3O_{6+x}$ from Ref.[42] (solid blue squares) and Ref.[3] (blue diamonds), with the $l = 1$ charge-density wave correlation length for $YBa_2Cu_3O_{6+x}$ from Ref.[42] (open blue squares), and with the charge-density wave correlation length for $HgBa_2CuO_{4+\delta}$ samples with $T_c = 72$ K (red) and 74 K (magenta) from Ref.[21]. The inset shows a schematic of a reconstructed electron pocket with grey shading representing the region of area broadening associated with ξ_{CDW}.

dominating the total spectral weight (i.e. momentum-space integrated intensity).[42,43] The other onsets only at high magnetic fields, is strictly uniaxial, is not staggered between consecutive layers (i.e. $l = 1$), has a longer correlation length but has lower total spectral weight (i.e. momentum-space integrated intensity). Equation (10) is found to be in reasonable only with the $l = \frac{1}{2}$ biaxial charge-density, which is consistent with it having a CuO_2-planar origin. The experimental ξ_{CDW} error bars are, however, very large, suggesting the need to extend x-ray scattering measurements to higher magnetic fields so as to achieve overlap with the regime over which magnetic quantum oscillations are observed. Other factors, such as oxygen chain ordering, could be at play in determining the longer correlation length of the substantially weaker $l = 1$ uniaxial charge-density wave.[42,43]

IV. DISCUSSION AND CONCLUSION

Having considered a scenario in which antiferromagnetism coexists with a biaxial charge-density density wave, we find that the single Fermi surface pocket is robust against short range fluctuations in the ordering vector of the antiferromagnetic order. The biaxial charge-density wave gaps states along the antiferromagnetic Brillouin zone boundary that would otherwise be heavily broadened by antiferromagnetic fluctuations. The relative insensitivity of the reconstructed electron pocket area to changes in the antiferromagnetic ordering vector causes this pocket to be protected against spatial antiferromagnetic fluctuations.

Using published values for the antiferromagnetic correlation lengths (i.e. $\xi \sim 10$ and 20 Å),[30,36–38,40] we find the small degree of residual broadening of the reconstructed electron pocket Landau level states is consistent with the magnetic field-dependence of the quantum oscillation amplitudes in two different families of underdoped cuprates – namely $YBa_2Cu_3O_{6+x}$ and $HgBa_2CuO_{4+\delta}$.[6,41] Our simulations suggest that the overall Landau level broadening is attributed mostly to spatial antiferromagnetic fluctuations, whose shorter ξ in $HgBa_2CuO_{4+\delta}$ compared to $YBa_2Cu_3O_{6+x}$ leads to a considerably greater damping of the quantum oscillation amplitude. The magnetic field-dependence of the Landau level broadening implies that the degree of damping of the quantum oscillations was likely to have been overestimated in prior experimental studies.

The ability of a biaxial charge-density wave to produce coherent Landau levels in the presence of short range antiferromagnetic fluctuations, especially under a strong magnetic field, suggests that the resilience of the electron pocket to antiferromagnetic fluctuations is likely to be an important factor in determining the high magnetic field ground state of the underdoped cuprates $YBa_2Cu_3O_{6+x}$ and $HgBa_2CuO_{4+\delta}$. Since charge-density waves are driven by interactions at the Fermi surface, the residual broadening of the electron pocket quasiparticle states also places limitations of the ability of the charge-density wave to acquire long range order. We show that the published values of the charge-density wave correlation length[3,21,42] are consistent with such a scenario, although subject to considerable experimental uncertainty.

Thus far we have considered a quasistatic approximation for the antiferromagnetic fluctuations, based on their reported low frequency in nuclear magnetic resonance measurements.[30] Of interest for future studies will be the question of whether the quantum oscillation amplitude is affected by temporal aspects of the antiferromagnetic fluctuations.

V. ACKNOWLEDGEMENTS

This work was supported by the US Department of Energy "Science of 100 tesla" BES program.

VI. APPENDIX

After Andersen *et al.*[44], we use the parameterization $\varepsilon = \varepsilon_0 + 2t_{10}[\cos ak_x + \cos bk_y] + 2t_{11}[\cos(ak_x + bk_y) + \cos(ak_x - bk_y)] + 2t_{20}[\cos 2ak_x + \cos 2bk_y]$, with a total band width $8t_{10} = 3$ eV and next nearest neighbor hoppings $t_{11}/t_{10} = -0.32$ and $t_{20}/t_{10} = 0.16$. All throughout the calculations, the chemical potential μ is adjusted to yield band fillings compatible with a total of $1+p$ holes, where p is the hole doping defined relative to the antiferromagnetic Mott insulator. Since we do not include the effect of the magnetic field on the band structure, we neglect the spin degrees of freedom.

We calculate the reconstructed energy bands of a $\delta = \frac{1}{3}$ biaxial charge-density wave, using the Hamiltonian

$$H_{\mathbf{k}}^{3\times 3\mathrm{CDW}} = \begin{pmatrix} \varepsilon_{\mathbf{k}} & V^d_{\mathbf{k}+\mathbf{Q}_x/2} & 0 & V^d_{\mathbf{k}+\mathbf{Q}_y/2} & 0 & 0 & \cdots \\ V^d_{\mathbf{k}+\mathbf{Q}_x/2} & \varepsilon_{\mathbf{k}+\mathbf{Q}_x} & V^d_{\mathbf{k}+3\mathbf{Q}_x/2} & 0 & V^d_{\mathbf{k}+\mathbf{Q}_y/2+\mathbf{Q}_x} & 0 & \cdots \\ 0 & V^d_{\mathbf{k}+3\mathbf{Q}_x/2} & \varepsilon_{\mathbf{k}+2\mathbf{Q}_x} & 0 & 0 & V^d_{\mathbf{k}+\mathbf{Q}_y/2+2\mathbf{Q}_x} & \cdots \\ V^d_{\mathbf{k}+\mathbf{Q}_y/2} & 0 & 0 & \varepsilon_{\mathbf{k}+\mathbf{Q}_y} & V^d_{\mathbf{k}+\mathbf{Q}_y+\mathbf{Q}_x/2} & 0 & \cdots \\ 0 & V^d_{\mathbf{k}+\mathbf{Q}_y/2+\mathbf{Q}_x} & 0 & V^d_{\mathbf{k}+\mathbf{Q}_y+\mathbf{Q}_x/2} & \varepsilon_{\mathbf{k}+\mathbf{Q}_y+\mathbf{Q}_x} & V^d_{\mathbf{k}+\mathbf{Q}_y+3\mathbf{Q}_x/2} & \cdots \\ 0 & 0 & V^d_{\mathbf{k}+\mathbf{Q}_y/2+2\mathbf{Q}_x} & 0 & V^d_{\mathbf{k}+\mathbf{Q}_y+3\mathbf{Q}_x/2} & \varepsilon_{\mathbf{k}+\mathbf{Q}_y+2\mathbf{Q}_x} & \cdots \\ \vdots & \vdots & \vdots & \vdots & \vdots & \vdots & \ddots \end{pmatrix}, \qquad (11)$$

which is a 9th rank tensor for $\delta = \frac{1}{3}$. After Allais *et al.*[12], we consider the charge-density wave potential to be of the $d_{x^2-y^2}$ form using the notation $V^d_{\mathbf{k}+n\mathbf{Q}_x+m\mathbf{Q}_y} = V_{\mathrm{CDW},0} d_{\mathbf{k}+n\mathbf{Q}_x+m\mathbf{Q}_y}$. Here, $d_{\mathbf{k}}$ is the d-wave form factor, $V_{\mathrm{CDW},0} = 0.2t_{10}$ is its magnitude while $n\mathbf{Q}_x + m\mathbf{Q}_y$ represents the its relative k-space position vector of the d-wave form factor for each matrix element.

To calculate the reconstructed Fermi surface resulting

solely from antiferromagnetic order, we use

$$H_{\mathbf{k}}^{\mathrm{AFM}} = \begin{pmatrix} \varepsilon_{\mathbf{k}} & V^{\mathrm{AFM}} \\ V^{\mathrm{AFM}} & \varepsilon_{\mathbf{k}+\mathbf{Q}_{\mathrm{AFM}}} \end{pmatrix}, \tag{12}$$

in which case there are only two reconstructed bands. Here, we use a uniform antiferromagnetic potential $V^{\mathrm{AFM}} = 0.5t_{10}$.

To combine antiferromagnetic and charge-density wave order, we nest $H_{\mathbf{k}}^{3\times3\mathrm{CDW}}$ with the antiferromagnetic Hamiltonian so as to obtain

$$H_{\mathbf{k}}^{\mathrm{AFM+CDW}} = \begin{pmatrix} H_{\mathbf{k}}^{3\times3\mathrm{CDW}} & I^9 V^{\mathrm{AFM}} \\ I^9 V^{\mathrm{AFM}} & H_{\mathbf{k}+\mathbf{Q}_{\mathrm{AFM}}}^{3\times3\mathrm{CDW}} \end{pmatrix}, \tag{13}$$

where I^9 is the 9^{th} rank identity matrix. Full diagonalization yields 18 bands, which roughly consist of two sets of 9 bands separated in energy.

[1] T. Wu, H. Mayaffre, S. Kramer, M. Horvatic, C. Berthier, W. N. Hardy, R. X. Liang, D. A. Bonn, M. H. Julien, Nature **477**, 191 (2011).

[2] G. Ghiringhelli, M. Le Tacon, M. Minola, S. Blanco-Canosa, C. Mazzoli, N. B. Brookes, G. M. De Luca, A. Frano, D. G. Hawthorn, F. He, T. Loew, M. Moretti Sala, D. C. Peets, M. Salluzzo, E. Schierle, R. Sutarto, G. A. Sawatzky, E. Weschke, B. Keimer, L. Braicovich, Science **337**, 821 (2012).

[3] J. Chang, E. Blackburn, A. T. Holmes, N. B. Christensen, J. Larsen, J. Mesot, Ruixing Liang, D. A. Bonn, W. N. Hardy, A. Watenphul, M. v. Zimmermann, E. M. Forgan, S. M. Hayden, Nature Phys. **8**, 871 (2012).

[4] S. E. Sebastian, N. Harrison, G. G. Lonzarich, Rep. Prog. Phys. **75**, 102501 (2012).

[5] S. E. Sebastian, N. Harrison, F. F. Balakirev, M. M. Altarawneh, P. A. Goddard, Ruixing Liang, D. A. Bonn, W. N. Hardy, G. G. Lonzarich, Nature **511**, 61 (2014).

[6] M. K. Chan, N. Harrison, R. D. McDonald, B. J. Ramshaw, K. A. Modic, N. Barisic, M. Greven, Nature Commun. **7**, 12244 (2016).

[7] D. LeBoeuf, S. Kramer, W. N. Hardy, R. X. Liang, D. A. Bonn, and C. Proust, Nat. Phys. **9**, 79 (2013).

[8] B. J. Ramshaw, N. Harrison, S. E. Sebastian, S. Ghannadzadeh, K. A. Modic, D. A. Bonn, W. N. Hardy, Ruixing Liang, P. A. Goddard, Quantum Materials **2**, 8 (2017).

[9] O. Cyr-Choinière, S. Badoux, G. Grissonnanche, B. Michon, S. A. A. Afshar, S. Fortier, D. LeBoeuf, D. Graf, J. Day, D. A. Bonn, W. N. Hardy, R. Liang, N. Doiron-Leyraud, L. Taillefer, Phys. Rev. X **7**, 031042 (2017).

[10] N. Harrison, S. E. Sebastian, Phys. Rev. Lett. **106**, 226402 (2011).

[11] A. V. Maharaj, P. Hosur, S. Raghu, Phys. Rev. B **90**, 125108 (2014).

[12] A. Allais, D. Chowdhury, S. Sachdev, Nature Commun. DOI: 10.1038/ncomms6771 (2014).

[13] A. K. R. Briffa, E. Blackburn, S. M. Hayden, E. A. Yelland, M. W. Long, E. M. Forgan, Phys. Rev. B **93**, 094502 (2016).

[14] N. Doiron-Leyraud, C. Proust, D. LeBoeuf, J. Levallois, B. Bonnemaison, R. X. Liang, D. A. Bonn, L. Taillefer, Nature **447**, 565 (2007).

[15] E. A. Yelland, J. Singleton, C. H. Mielke, N. Harrison, F. F. Balakirev, B. Dabrowski, J. R. Cooper, Phys. Rev. Lett. **100**, 047003 (2008).

[16] N. Barišić, S. Badoux, M. K. Chan, C. Dorow, W. Tabis, B. Vignolle, G. Yu, Jérôme Béard, X. Zhao, C. Proust, M. Greven, Nature Phys. **9**, 761-764 (2013).

[17] D. LeBoeuf, N. Doiron-Leyraud, J. Levallois, R. Daou, J.-B. Bonnemaison, N. E. Hussey, L. Balicas, B. J. Ramshaw, R. Liang, D. A. Bonn, W. N. Hardy, S. Adachi, C. Proust, L. Taillefer, Nature **450**, 533 (2007).

[18] N. Harrison, S. E. Sebastian, On the relationship between charge ordering and the Fermi arcs observed in underdoped high T_{c} superconductors, New J. Phys. **16**, 063025 (2014).

[19] R. Comin, A. Frano, M. M. Yee, Y. Yoshida, H. Eisaki, E. Schierle, E. Weschke, R. Sutarto, F. He, A. Soumyanarayanan, Y. He, M. Le Tacon, I. S. Elfimov, J. E. Hoffman, G. A. Sawatzky, B. Keimer, A. Damascelli, Science **343**, 390 (2014).

[20] S. Blanco-Canosa, A. Frano, E. Schierle, J. Porras, T. Loew, M. Minola, M. Bluschke, E. Weschke, B. Keimer, M. Le Tacon Phys. Rev. B **90**, 054513 (2014).

[21] W. Tabis, B. Yu, I. Bialo, M. Bluschke, T. Kolodziej, A. Kozlowski, E. Blackburn, K. Sen, E. M. Forgan, M. v. Zimmermann, Y. Tang, E. Weschke, B. Vignolle, M. Hepting, H. Gretarsson, R. Sutarto, F. He, M. Le Tacon, N. Barisic, G. Yu, M. Greven, Phys. Rev. B **96**, 134510 (2017).

[22] M. R. Norman, H. Ding, M. Randeria, J. C. Campuzano, T. Yokoya, T. Takeuchi, T. Takahashi, T. Mochiku, K. Kadowaki, P. Guptasarma, D. G. Hinks, Destruction of the Fermi surface in underdoped high-Tc superconductors, Nature **392**, 157 - 160 (1998).

[23] W. A. Atkinson,A. P. Kampf, S. Bulut, New J. Phys. **17**m 013025 (2015).

[24] N. Harrison, Phys. Rev. B **94**, 085129 (2016).

[25] L. Zhang, J.-W. Mei, Europhys. Lett. **114**, 47008 (2016).

[26] L. Zhang, J.-W. Mei, preprint arXiv:1408.6592 (2014).

[27] F. F. Balakirev. J. B. Betts, A. Migliori, S. Ono, Y. Ando, G. S. Boebinger, Nature **424**, 912-915 (2003).

[28] Y. Ando, Y. Kurita, S. Komiya, S. Ono, K. Segawa, Phys. Rev. Lett. **92**, 197001 (2004).

[29] S. Badoux, W. Tabis, F. Laliberté, G. Grissonnanche, B. Vignolle, D. Vignolles, J. Béard, D. A. Bonn, W. N. Hardy, R. Liang, N. Doiron-Leyraud, L.Taillefer, C. Proust, Nature **531**, 210-214 (2016).

[30] A. P. Kampf, Phys. Rep. **249**, 219-351 (1994).

[31] N. Harrison, R. D. McDonald, J. Singleton, Phys. Rev. Lett. **99**, 206406 (2007).

[32] E. Z. Kuchinskii and M. V. Sadovskii, JETP Letters **88**, 192 - 196 (2008).

[33] M. R. Norman, A. Kanigel, M. Randeria, U. Chatterjee, and J. C. Campuzano, Phys. Rev. B **76**, 174501 (2007).

[34] M. A. Hossain, J. D. F. Mottershead, D. Fournier, A. Bostwick, J. L. McChesney, E. Rotenberg, R. Liang, W. N. Hardy, G. A. Sawatzky, I. S. Elfimov, D. A. Bonn, A. Damascelli Nature Phys. **4**, 527 (2008).

[35] D. Shoenberg, *Magnetic Oscillations in Metals* (Cambridge

University Press, 1984).
[36] C. Stock, W. J. L. Buyers, R. A. Cowley, P. S. Clegg, R. Coldea, C. D. Frost, R. Liang, D. Peets, D. Bonn, W. N. Hardy, R. J. Birgeneau, Phys. Rev. B **71**, 024522 (2005).
[37] H. Monien, D. Pines, M. Takigawa, Phys. Rev. B. **43**, 258-274 (1991)
[38] T.E. Mason, G. Aeppli and H.A. Mook, Phys. Rev. Lett. **68**, 1414, 1992.
[39] B. J. Ramshaw, S. E. Sebastian, R. D. McDonald, James Day, B. S. Tan, Z. Zhu, J. B. Betts, Ruixing Liang, D. A. Bonn, W. N. Hardy, N. Harrison, Science **348**, 317 (2015).
[40] M. K. Chan, C. J. Dorow, L. Mangin-Thro, Y. Tang, Y. Ge, M. J. Veit, G. Yu, X. Zhao, A. D. Christianson, J. T. Park, Y. Sidis, P. Steffens, D. L. Abernathy, P. Bourges, M. Greven, Nature Commun. **7**, 10819 (2016).
[41] S. E. Sebastian, N. Harrison, M.M. Altarawneh, Ruixing Liang, D.A. Bonn, W.N. Hardy, G.G. Lonzarich Nature Commun. **2**, 471 (2011).
[42] S. Gerber, H. Jang, H. Nojiri, S. Matsuzawa, H. Yasumura, D. A. Bonn, R. Liang, W. N. Hardy, Z. Islam, A. Mehta, S. Song, M. Sikorski, D. Stefanescu, Y. Feng, S. A. Kivelson, T. P. Devereaux, Z.-X. Shen, C.-C. Kao, W.-S. Lee, D. Zhu, J.-S. Lee, Science **350**, 949 (2015).
[43] H. Jang, W.-S. Lee, H. Nojiri, S. Matsuzawa, H. Yasumura, L. Nie, A. V. Maharaj, S. Gerber, Y.-J. Liu, A. Mehta, D. A. Bonn, R. Liang, W. N. Hardy, C. A. Burns, Z. Islam, S. Song, J. Hastings, T. P. Devereaux, Z.-X. Shen, S. A. Kivelson, C.-C. Kao, D. Zhu, J.-S. Lee, Proceedings of the National Academy of Sciences **113**, 14645-14650, (2016).
[44] O. K. Andersen, A. I. Liechtenstein, O. Jepsen, and F. Paulsen, J. Phys. Chem. Solids **56**, 1573 (1995).